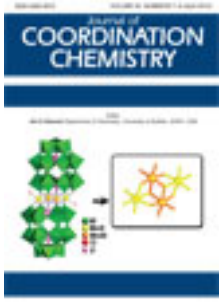

Journal of Coordination Chemistry
Publication details, including instructions for authors and subscription information:
http://www.tandfonline.com/loi/gcoo20

A thermodynamic and kinetic study on $[PdCl_4]^{2-}$ complex formation with L-cystine

Alexander I. Petrov [a] , Nicolay N. Golovnev [a] & Alexander A. Leshok [a]

[a] Institute of Non-Ferrous Metals and Materials Science, Siberian Federal University , Krasnoyarsk , Russian Federation

Published online: 23 Mar 2012.

To cite this article: Alexander I. Petrov , Nicolay N. Golovnev & Alexander A. Leshok (2012) A thermodynamic and kinetic study on $[PdCl_4]^{2-}$ complex formation with L-cystine, Journal of Coordination Chemistry, 65:8, 1339-1353, DOI: 10.1080/00958972.2012.672733

To link to this article: http://dx.doi.org/10.1080/00958972.2012.672733

Journal of Coordination Chemistry
Vol. 65, No. 8, 20 April 2012, 1339–1353

Taylor & Francis
Taylor & Francis Group

A thermodynamic and kinetic study on $[PdCl_4]^{2-}$ complex formation with L-cystine

ALEXANDER I. PETROV*, NICOLAY N. GOLOVNEV and ALEXANDER A. LESHOK

Institute of Non-Ferrous Metals and Materials Science, Siberian Federal University, Krasnoyarsk, Russian Federation

(*Received 18 September 2011; in final form 8 February 2012*)

Complex formation of $PdCl_4^{2-}$ with L-cystine (H_2CysS) has been studied in hydrochloric aqueous solutions (0.05–1 mol L^{-1} HCl) by UV-Vis spectroscopy combined with quantum chemical calculations. Our data suggest that L-cystine acts as a monodentate S-coordinating ligand in highly acidic solutions and no evidence of S–S bond fission was found to occur under the experimental conditions. Thermodynamic parameters for $Pd(H_4CysS)Cl_3^+$ formation were determined: the monocomplex stability constant $\log K_1 = 3.3$ (298 K), $\Delta H = -27\,kJ\,mol^{-1}$, and $\Delta S = -29\,JK^{-1}mol^{-1}$ (0.5 mol L^{-1} HCl). The experimental reaction rate law has been obtained: $W = k[H_4CysS^{2+}][PdCl_4^{2-}][Cl^-]^{-0.86}$ and the values for the activation parameters have been determined: $E_a = 66\,kJ\,mol^{-1}$, $\Delta H^1 = 63\,kJ\,mol^{-1}$, and $\Delta S^1 = -77\,JK^{-1}mol^{-1}$. The electronic absorption spectra (EAS) of the $Pd(H_4CysS)Cl_3^+$ complex were computed using time-dependent density functional theory and the polarizable continuum model. The def2-TZVPP basis set (PBE0 and TPSS density functionals) provides good agreement between the experimental and theoretical EAS.

Keywords: Palladium(II); Cystine; Kinetics; DFT; TD-DFT

1. Introduction

It is important to study kinetics, mechanisms, and thermodynamics of ligand exchange processes in square-planar complexes of Pd(II) and other platinum metal ions since such complexes are widely used in applied chemistry, catalysis, and medicine [1, 2]. S-donor amino acids like L-cystine (H_2CysS, dicysteine) possess strong affinity to platinum metal ions and form complexes with cisplatin [3] and with $PdCl_4^{2-}$ [4]. Thus findings on complex formation of S-donor ligands with Pd(II) and other "soft" Lewis acids are important for prediction of their behavior in aqueous solutions including biological systems.

$[PdCl_4]^{2-}$ has been suggested as an analytical reagent for the determination of C–S–S–C ligands [5]. The S–S bond appears to be quite strong, undergoing fission only in boiling solutions of H_2CysS and $[PdCl_4]^{2-}$, and leading to formation of the palladium-cysteine complex $Pd(HCys)_2$. Thus the probability of S–S bond fission in cystine

*Corresponding author. Email: sfupetrov@gmail.com

ISSN 0095-8972 print/ISSN 1029-0389 online
http://dx.doi.org/10.1080/00958972.2012.672733

solutions is negligible at room temperature [6]. Our article deals with strongly acidic solutions, therefore L-cystine should be considered an S-donor ligand being potentially selective to platinum metals since the S–S group commonly possesses weaker electron donor properties than the thiol group. Thus studies of complex formation of disulfide ligands with platinum metals may result in significant advances in platinum metal chemistry.

Recently we reported [4] that the interaction of $PdCl_4^{2-}$ with L-cystine leads to $Pd(H_4CysS)Cl_3^+$ formation:

$$PdCl_4^{2-} + H_4CysS^{2+} \overset{K_1}{\rightleftharpoons} Pd(H_4CysS)Cl_3^+ + Cl^- \quad (1)$$

This research was conducted at palladium concentration (C_{Pd}) exceeding cystine concentration (C_{CysS}) to avoid formation of complexes other than $Pd(H_4CysS)Cl_3^+$. A set of apparent stability constants was obtained ($[Cl^-] = 1.0$, 0.5, and 0.25 mol L^{-1}; $[H^+] = 0.10$–1.00 mol L^{-1}) and analyzed in terms of acidity and chloride concentration effects on the apparent stability constant K_{app}. Earlier we suggested [4] monodentate Pd(II) coordination to a sulfur of disulfide group since K_{app} did not depend on $[H^+]$, and the coordinating properties of $-COOH$ and $-NH_3^+$ groups were reduced in strongly acidic solutions. On the other hand, the dependence of $K_{app} = K_1 \cdot [Cl]^{-1}$ gave evidence that only one chloride was substituted by an incoming cystine ligand.

This article is focused on a spectrophotometric study of the $PdCl_4^{2-}$ interaction with H_4CysS^{2+} in hydrochloric aqueous solutions and on the determination of both kinetic and thermodynamic parameters. The new set of K_{app} values has been obtained at various acidities, chloride concentration levels, and temperatures; values of formation enthalpy and entropy have also been determined.

2. Experimental

2.1. *The chemicals*

All chemicals were of analytical grade: HCl, $C_6H_{12}N_2S_2O_4$ (cystine, 99%, Aldrich), $HClO_4$, Na_2CO_3, and NaCl. A stock solution of K_2PdCl_4 was prepared according to standard practice [4]. The $NaClO_4$ solution was obtained by neutralization of Na_2CO_3 with perchloric acid. The concentration of sodium perchlorate was determined gravimetrically as Na_2SO_4. An accurate weight of $NaClO_4$ was dissolved in 1 mL of concentrated sulfuric acid, this solution was then evaporated and the dry salt was subsequently calcined at 650°C to constant mass. Concentrations of HCl and $HClO_4$ were determined titrimetrically with standardized Na_2CO_3 solution. The NaCl (2 mol L^{-1}) and cystine (0.005 mol L^{-1}) solutions were obtained by dissolution of their accurate weights. The cystine stock solution also contained 0.5 mol L^{-1} HCl.

2.2. *Equipment*

UV-Vis spectra were measured with an Evolution 300 scanning spectrophotometer (ThermoScientific, England) using 1 cm quartz cells. Cell thermostating (±0.1 K) was performed with a Haake K15 thermostat connected to a Haake DC10 controller.

2.3. *Equilibrium studies*

The determination technique of K_{app} and "true" K_1 stability constants has been already described in our previous paper [4]. The concentration of L-cystine (C_{CysS}) was maintained constant (usually 5×10^{-5} mol L^{-1}) and the concentration of $[PdCl_4]^{2-}$ (C_{Pd}) was varied from 3×10^{-4} mol L^{-1} up to 1×10^{-3} mol L^{-1} throughout the experiments. The required acidity ($C_H = 0.2$–2 mol L^{-1}) was provided with HCl and $HClO_4$ and ionic strength ($I = 0.2$–2) was maintained with NaCl and $NaClO_4$. The series of reactant solutions were prepared from previously thermostated (±0.1 K) stock reagent solutions which had been kept in the dark for 18 h (±0.1 K). Their absorbance was measured over the 220–450 nm range after such equilibration.

2.4. *Kinetic measurements*

Formation kinetics of $Pd(H_4CysS)Cl_3^+$ were followed at 385 nm. Every solution and distilled water was thermostated (±1 K) before the experiment. The reaction was initiated by rapid addition of the required cystine solution volume into the flask containing palladium(II) and the background mixed medium solution. The volume of the initiated reacting solution was quickly adjusted with distilled water. The flask was rapidly stirred and the solution was poured into the thermostated (±0.1 K) cell. The progress of reaction was followed by continuous absorbance measurements in the automatic mode. C_{Pd} varied from 5×10^{-4} mol L^{-1} to 2.5×10^{-3} mol L^{-1}. C_{CysS} varied from 2×10^{-5} mol L^{-1} to 1.25×10^{-4} mol L^{-1}. Absorbance measurement was conducted at 385 nm every 5 sec for 10 min from the moment the reaction had been initiated and these data were used to determine reaction orders with respect to reagents and rate constants. Every kinetic experiment was performed in triplicate: reaction orders, reaction rate constants, and activation parameters were averaged.

2.5. *Quantum chemical calculations*

Calculations were carried out using the GAMESS US program package [7]. Geometry optimization was performed by density functional theory (DFT) with the hybrid functional TPSS under Grimme's empirical correction with no symmetry constraints. The basis set def2-TZVPP was applied to every atom in the complex during every computational procedure. Vertical excitation energies were computed for the first 21 singlet excited states to reproduce the UV-Vis spectra of complexes (PBE0 and TPSS functionals). Solvent effects were evaluated using the non-equilibrium implementation of the conductor-like polarizable continuum model (C-PCM), built-in parameters for water being the solvent were used. A 1.63 Å Van-der-Waals atomic radius was used for Pd, built-in radii were assigned to the other atoms. The calculated absorption energies and intensities were transformed with the GabEdit program into simulated spectra [8]. Lorentian functions were used assuming a constant bandwidth at the half-height of 12 nm. The simulated spectrum was renormalized with respect to the maximum oscillator strength. The optimized geometries were visualized with ChemCraft software [9] as were the molecular orbitals. Their percentage compositions were found with QMForge software [10].

3. Results and discussion

3.1. *Thermodynamics*

The distribution diagrams were calculated before [11–14] for the $Pd(H_2O)_{4-i}Cl_i^{2-i}$ and H_nCysS^{n-2} species. They gave evidence of $PdCl_4^{2-}$ and H_4CysS^{2+} being the only dominant species under the specified conditions. Hence the reaction between $PdCl_4^{2-}$ and H_4CysS^{2+} can be described as in equation (1).

UV-Vis spectra were used as raw data for the calculation of absorbance changes due to complex formation ΔA [4]. Figure 1 shows a typical ΔA–λ plot for a set of process solutions. These data were obtained from seven process solutions with the same C_{CysS} and different C_{Pd}. Tables S1–S3 provide a full set of ΔA values (Supplementary material).

The ΔA–λ plots had the same nature throughout the study and the maximum at 317 nm did not change its wavelength at different C_{Pd}. This fact together with the $C_{Pd} > C_{CysS}$ condition agreed with only mononuclear mono-complex formation. The K_{app} values (K_{app} is expressed without taking the chloride concentration into account) that were obtained in this study and in our recent study [4] are combined in table 1. As seen from table 1, the new K_{app} values fit equation (1) perfectly. Here and throughout the entire article the "±" values represent confidence limits given for the 95% confidence level.

These data indicate S-coordination of H_4CysS^{2+} since changes in acidity do not affect the K_{app} values. The K_1 value calculated from the set of K_{app} at different $[Cl^-]$ levels and 298 K ($\log K_1 = 3.4 \pm 0.1$, $I = 0.5$; $\log K_1 = 3.2 \pm 0.1$, $I = 1$) is invariant, and we suggest that only one chloride in $PdCl_4^{2-}$ is substituted by the cystine ligand. $Pd(H_4CysS)Cl_3^+$ is the only product within the broad range of $[H^+]$ and $[Cl^-]$, but in 0.05 mol L^{-1} HCl + 0.45 mol L^{-1} NaCl, cystine apparently turns to a S, N- or S, N,O-coordinating ligand. ΔH and ΔS values are -27 ± 2 kJ mol^{-1} and -29 ± 3 JK^{-1} mol^{-1}, respectively

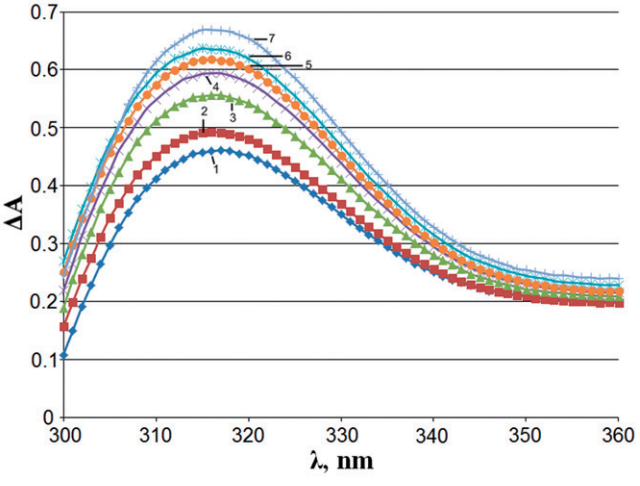

Figure 1. Plot of ΔA *vs.* λ at different $C_{Pd} \times 10^4$ mol L^{-1}: 3.00 (1); 4.00 (2); 5.00 (3); 6.00 (4); 7.00 (5); 8.00 (6); 9.00 (7). $C_{CysS} = 5 \times 10^{-5}$ mol L^{-1}. $C_{HCl} = 0.5$ mol L^{-1}. $I = 0.5$. 298 K.

Table 1. Apparent (K_{app}) and "true" (K_1) stability constants of $Pd(H_4CysS)Cl_3^+$ monocomplex.

I	Ionic background (mol L^{-1})	T (K)	log K_{app}	log K_1
0.2	0.2 HCl	298	3.94 ± 0.05	3.24
0.25	0.25 HCl	298	3.80 ± 0.02	3.20
0.5	0.5 HCl	278	3.90 ± 0.09*	3.60
		288	3.74 ± 0.04	3.44
		298	3.61 ± 0.06*	3.31
		313	3.30 ± 0.06*	3.00
		333	3.08 ± 0.08	2.78
	0.25 HCl + 0.25 NaCl	298	3.55 ± 0.06	3.25
	0.25 HCl + 0.25 $HClO_4$	298	3.86 ± 0.06*	3.26
	0.05 HCl + 0.45 NaCl	298	3.81 ± 0.03	3.51
1	1 HCl	298	3.22 ± 0.04	3.22
	0.5 HCl + 0.5 NaCl	298	3.14 ± 0.04	3.14
	0.5 HCl + 0.5 $HClO_4$	298	3.55 ± 0.05	3.25
2	1 HCl + 1 $HClO_4$	298	2.99 ± 0.04	2.99

*Values taken from [4].

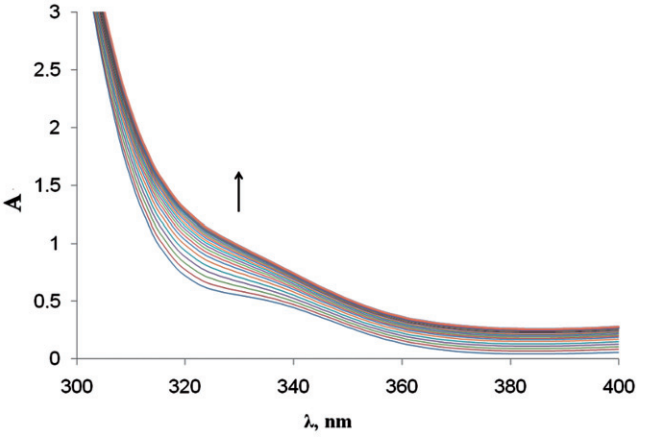

Figure 2. Spectroscopic changes that occurred during reaction of $[PdCl_4]^{2-}$ with L-cystine ($C_{Pd} = 1 \times 10^{-3}$ mol L^{-1}, $C_{CysS} = 7.5 \times 10^{-5}$ mol L^{-1}, 0.5 mol L^{-1} HCl, 298 K, $t = 330$ s).

(0.5 mol L^{-1} HCl). Thus the enthalpy makes the crucial contribution at 298 K. Such behavior is common for "soft" S-donor ligands.

3.2. *Kinetics*

3.2.1. Determination of reaction orders. The reaction order with respect to cystine was determined following the pseudo-first-order approach ($C_{Pd} > C_{CysS}$). Figure 2 shows the changes in the UV-Vis spectra during complex formation of $[PdCl_4]^{2-}$ with cystine. Here we should note that the values of log K_{app} obtained at 317 nm (table 1) and 385 nm coincided within the limits of the experimental error, thus confirming our K_{app} value.

Complex absorptivity value $\varepsilon_1 = 5000 \pm 310$ was determined at 385 nm in 0.5 mol L^{-1} HCl and has been used throughout the further studies and calculations.

The concentration of $Pd(H_4CysS)Cl_3^+$ (C_{PdCysS}) was calculated from the following equation:

$$C_{PdCysS} = \frac{A_t - A_{Pd}}{\varepsilon_1}, \tag{2}$$

where A_t and A_{Pd} are absorbances of the $PdCl_4^{2-}$ solution with and without cystine present, respectively. In spite of inherent $PdCl_4^{2-}$ absorptivity at 385 nm being insignificant ($\varepsilon_{Pd} = 31$), its contribution to the total absorbance was taken into account at high C_{Pd}. Interference from cystine absorbance was negligible. The plots of C_{PdCysS} *versus* time are shown in figure 3.

The reaction orders with respect to reagents were determined using the initial reaction rate approach under pseudo-first-order conditions [15–17]. Reaction rate is expressed by equation (3). If $C_{Pd} \gg C_{CysS}$ the observed rate constant $k_{obs} = k \cdot C_{Pd}^m$, thus the reaction rate obeys equation (4).

$$W = \frac{dC_{PdCysS}}{dt} = kC_{CysS}^n C_{Pd}^m, \tag{3}$$

$$W = \frac{dC_{PdCysS}}{dt} = k_{obs} C_{CysS}^n. \tag{4}$$

Reaction rate W was determined from the initial linear part of the plot of C_{PdCysS} *versus* time ($t \leq 2$ min) by the least-squares fitting procedure (table S4 in "Supplementary material"). The highest possible error of reaction rate determination did not exceed 5%. Equation (4) was used for calculation of k_{obs} and the reaction order with respect to cystine (n). The reaction order for cystine and k_{obs} were found using curve fitting.

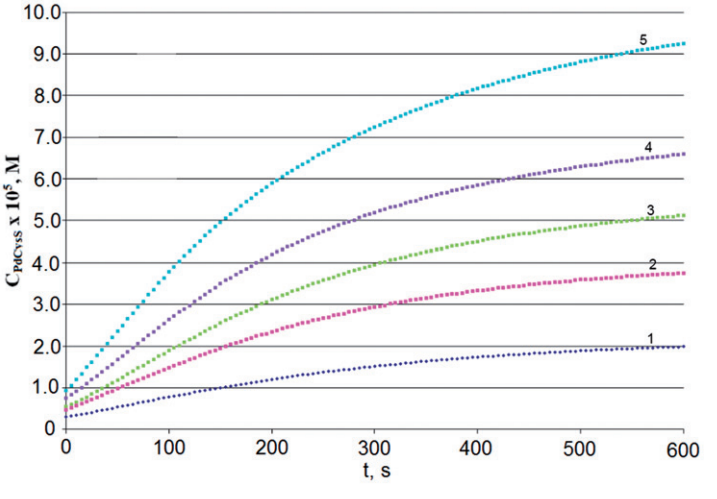

Figure 3. Pseudo-first-order kinetic plots for reaction of $[PdCl_4]^{2-}$ with L-cystine. Experimental conditions: $C_{Pd} = 1.1 \times 10^{-3}$ mol L^{-1} and $C_{CysS} \times 10^5$ mol $L^{-1} = 2$ (1), 4 (2), 6 (3), 8 (4), 12 (5). $C_{HCl} = 0.5$ mol L^{-1}. $I = 0.5$. 298 K.

Some kinetic runs were carried out at different C_{Pd} levels with C_{Pd} ranging from 5×10^{-4} to 2.5×10^{-3} mol L^{-1} to determine the reaction order with respect to $PdCl_4^{2-}$. The cystine concentration was maintained the same within each set (from 2×10^{-5} mol L^{-1} up to 1.2×10^{-4} mol L^{-1}). The observed pseudo-first-order reaction rate constant (k_{obs}) and n were determined from the W *versus* C_{CysS} plots which had been obtained at different palladium concentrations (figure 4). The k_{obs} values calculated for each C_{Pd} level are listed in table S5, "Supplementary material."

The corresponding plot is shown in figure 5. Calculations indicate that $m = 0.98 \pm 0.05$ and $\log k = 0.30 \pm 0.05$, thus collaterally supporting our suggestion of the mono-complex being the only product.

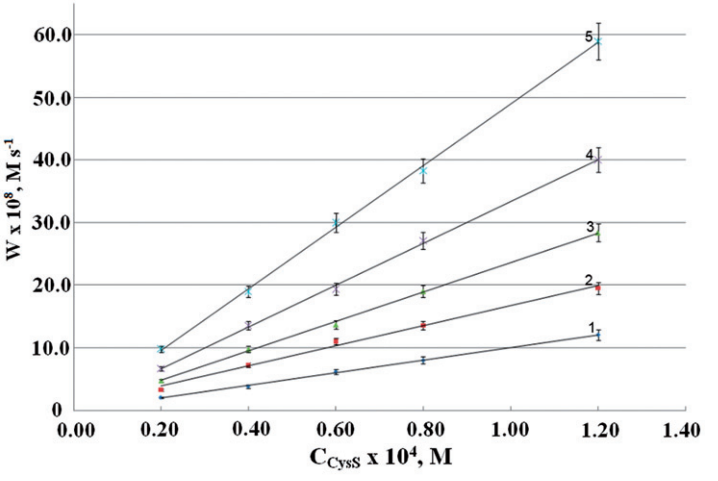

Figure 4. Plots of W *vs.* C_{CysS}. Experimental conditions: $C_{Pd} \times 10^{-3}$ mol L^{-1}: 0.5 (1); 0.75 (2); 1.1 (3); 1.7 (4); 2.5 (5). $C_{HCl} = 0.5$ mol L^{-1}. $I = 0.5$. 298 K.

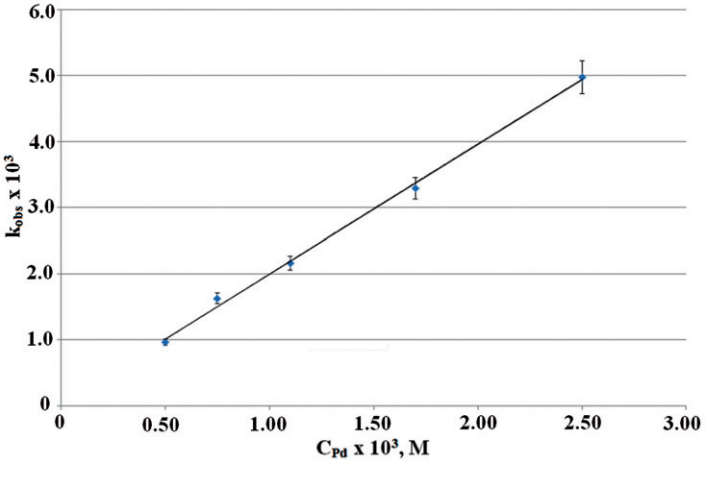

Figure 5. Plot of k_{obs} *vs.* C_{Pd}. $C_{HCl} = 0.5$ mol L^{-1}. $I = 0.5$. 298 K.

Table 2. Effect of $[Cl^-]$ on k_{obs}.

Ionic background ($mol\,L^{-1}$)	$0.2HCl + 0.8HClO_4$	$0.35HCl + 0.65HClO_4$	$0.5HCl + 0.5HClO_4$	$0.8HCl + 0.2HClO_4$	1HCl
$k_{obs} \cdot 10^2$, s^{-1}	1.02	0.59	0.50	0.31	0.27

Table 3. Simultaneous effect of $[H^+]$ and $[Cl^-]$ on k_{obs}.

Ionic background ($mol\,L^{-1}$)	$0.2HCl + 0.8NaClO_4$	$0.3HCl + 0.7NaClO_4$	$0.5HCl + 0.5NaClO_4$	$0.7HCl + 0.3NaClO_4$	1HCl
$k_{obs} \cdot 10^2$, s^{-1}	1.04	0.75	0.40	0.35	0.27

3.2.2. Effects of $[H^+]$ and $[Cl^-]$ on reaction rate. The following equation was used to study such effect:

$$\ln\left(\frac{A_0 - A_\infty}{A_i - A_\infty}\right) = k_{obs}t. \quad (5)$$

Here A_0, A_i, and A_∞ are the initial, current, and equilibrium absorbances of a studied solution. The effect of chloride concentration was studied at constant acidity $[H^+] = 1\,mol\,L^{-1}$ and ionic strength $I = 1$ ($HCl + HClO_4$). Table 2 shows the observed (pseudo-first-order) rate constants obtained at different chloride concentration levels ($C_{Pd} = 2.5 \times 10^{-3}\,mol\,L^{-1}$ and $C_{CysS} = 6 \times 10^{-5}\,mol\,L^{-1}$). Reaction rate decreases significantly at higher chloride concentrations. As seen from table 2 the C_{Cl}^{-p} multiplier should be inserted into the kinetic equation (2), where $p = 0.85 \pm 0.08$.

Both acid and chloride concentrations were varied simultaneously to check if any background acidity change would affect the reaction rate constant. These data are shown in table 3. The p value is nearly the same (0.86), thus such effect is insignificant and should be neglected. Actually there is no evidence that acidity affects the reaction rate constant within the range $[H^+] = 0.2$–$1\,mol\,L^{-1}$.

3.2.3. Determination of activation parameters. The kinetics were followed at four different temperatures 278, 288, 298, 308 K and $I = 0.5$; $[Cl^-] = 0.5\,mol\,L^{-1}$; $[H^+] = 0.5\,mol\,L^{-1}$. The mean k_{obs} values are listed in table S6, "Supplementary material." The rate constants increase at higher temperatures. The activation energy corresponding to these constants was evaluated from the Arrhenius plot of $\log k_{obs}$ *versus* $1/T$ ($R^2 = 0.993$). Activation enthalpy and entropy values were calculated using the Eyring equation. The values of the activation parameters are: $E_a = 66 \pm 4\,kJ\,mol^{-1}$, $\Delta H^{\ddagger} = 63 \pm 4\,kJ\,mol^{-1}$, $\Delta S^{\ddagger} = -77 \pm 7\,J\,K^{-1}\,mol^{-1}$ (the $\pm$ values represent 95% confidence limits).

These activation parameters are quite close to those previously determined [18] for the reaction of $[PdCl_4]^{2-}$ with ethylenediamine: $\Delta H^{\ddagger} = 85\,kJ\,mol^{-1}$, $\Delta S^{\ddagger} = -90\,JK^{-1}\,mol^{-1}$ [18].

3.3. *Discussion of the reaction mechanism*

The experimental rate law is

$$\frac{d[Pd(H_4CysS)Cl_3^+]}{dt} = k[H_4CysS^{2+}][PdCl_4^{2-}][Cl^-]^{-0.86}. \quad (6)$$

Square-planar Pd(II), Pt(II), and Ni(II) complexes tend to undergo two parallel reaction pathways (direct and solvation) resulting in a single product [19]. These pathways are presented in scheme 1.

The theoretical reaction rate law for scheme 1 was derived. Reversibility of each reaction step was taken into account, thus reflecting the theoretical model. The detailed derivation of this theoretical reaction rate law can be found in the appendix (Supplementary material); its simplified expression is

$$\frac{d[Pd(H_4CysS)Cl_3^+]}{dt} = k\frac{[PdCl_4^{2-}]}{[Cl^-]}[H_4CysS^{2+}]. \quad (7)$$

The solvation pathway (scheme 1) is the only case where such an inverse dependence of the reaction rate on $[Cl^-]$ can occur. Its first step leads to the formation of the less reactive trichloroaquapalladium(II) species, with consecutive H_2O substitution by H_4CysS^{2+} being the rate-limiting step, since the $[PdCl_4]^{2-}$ aquation rate constant exceeds our k_2 value by four times [14]. Therefore, our k_2 value should be ascribed to the reaction of $[PdCl_3(H_2O)]^-$ with H_4CysS^{2+}. The final stoichiometric reaction mechanism is shown in equations (8) and (9). Each step involves an associative mechanism (A).

$$PdCl_4^{2-} + H_2O \rightleftharpoons [PdCl_3OH_2]^- + Cl^-, \quad (8)$$

$$[PdCl_3OH_2]^- + H_4CysS^{2+} \rightleftharpoons Pd(H_4CysS)Cl_3^+ + H_2O \quad (9)$$

The same interpretation can be found in [18], whose authors studied the interaction of $[PdCl_4]^{2-}$ with ethylenediamine and reported an inverse dependence of the reaction rate on $[H^+]$ and $[Cl^-]$, namely asymptotic reaction rates which decrease at high $[H^+]$ and $[Cl^-]$ levels. Such an effect of $[H^+]$ was explained by the different reactivity of protonated ligand species, but no detailed explanation for the chloride concentration

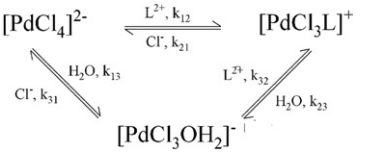

Scheme 1. Dual-route ligand substitution mechanism.

effect on reaction rate was provided. The reaction rate law was derived considering interaction of reacting species as irreversible.

Complex formation of different Pd(II) complexes with 8-oxyhinoline was studied [20] and suggested a possible explanation for the chloride concentration effect on the ligand substitution reaction rate for square-planar complexes of Pd(II). They reported a relatively low value for the effect of [Cl^-] (between 0.3 and 0.5) which may be ascribed to an I_d mechanism, while our relatively high value of 0.86 suggests an I_a mechanism. In spite of $\Delta S^{\ddagger}$ being negative (i.e., the system becomes more ordered), one is not able to choose a final reaction mechanism due to uncertainties arising from the effect of solvational changes of the charged species involved.

3.4. *DFT and TD-DFT computations*

Computational chemistry is a powerful tool enabling scientists to create and check different models representing real chemical objects and supporting experimental data. We performed a computational study (DFT/def2-TZVPP) involving geometry optimization of $Pd(H_4CysS)Cl_3^+$ (figure 6) and TD-DFT calculations allowing us to predict and to compare electronic absorption spectra (EAS) of Pd(II) complexes. Structural parameters (angles and bond lengths) of $Pd(H_4CysS)Cl_3^+$ are listed in table 4. The chosen functional and basis set provide error limits within an interval of ±0.02 Å.

According to experimental X-ray diffraction data, the S–S bond in free cystine is marginally shorter being 2.049 Å [21] compared to 2.088 Å in $Pd(H_4CysS)Cl_3^+$ (our DFT data). The dihedral C1–S1S2–C1 angle also widens from 89.6° (free cystine, XRD) to 122.0° in $Pd(H_4CysS)Cl_3^+$ (DFT). According to XRD, Pd–Cl and Pd–S distances are 2.30 Å and 2.34 Å, respectively [22, 23]. These values are in good agreement with our DFT data.

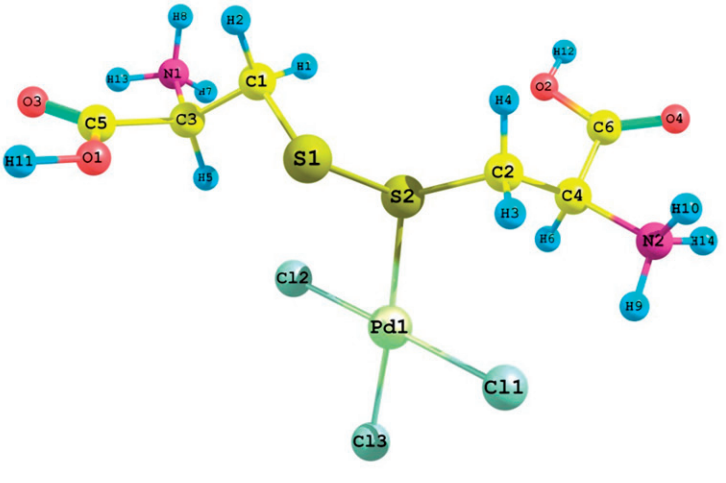

Figure 6. Optimized geometry of $Pd(H_4CysS)Cl_3^+$.

Table 4. Structural parameters of $Pd(H_4CysS)Cl_3^+$ geometry (DFT data).

Bond	Length (Å)	Angle	Value (°)
S1–S2	2.088	C1–S1–S2	99.9
S1–C1	1.835	C3–C1–S1	112.2
C1–C3	1.537	C5–C3–C1	111.3
C3–C5	1.536	N1–C3–C1	110.7
C3–N1	1.518	N1–C3–C5	110.3
C5–O1	1.331	C3–C5–O1	111.4
C5–O3	1.216	C3–C5–O3	122.7
Pd1–S2	2.277	O1–C5–O3	125.8
Pd1–Cl1	2.350	C2–S2–S1	98.6
Pd1–Cl2	2.336	C4–C2–S2	109.5
Pd1–Cl3	2.327	C6–C4–C2	115.4
S2–C2	1.841	N2–C4–C2	109.9
C2–C4	1.537	N2–C4–C6	108.1
C4–C6	1.526	C4–C6–O2	110.7
C4–N2	1.502	C4–C5–O4	123.0
C6–O2	1.335	O2–C6–O4	126.3
C6–O4	1.214	C1–S1–S2–C2	122.0

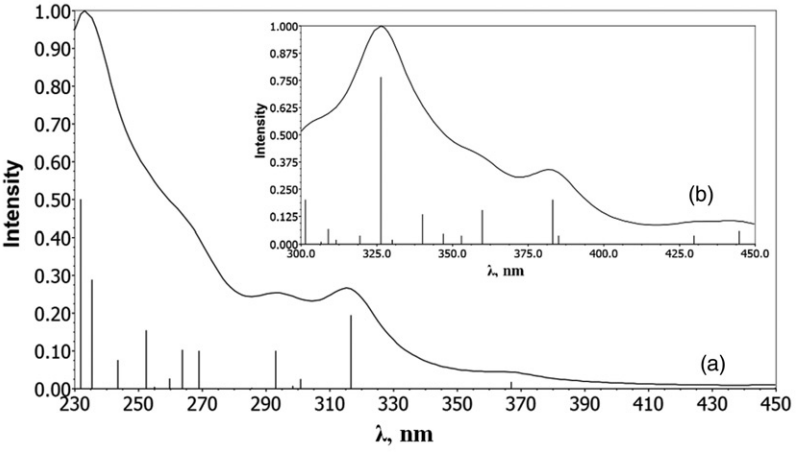

Figure 7. TD-DFT EAS of $Pd(H_4CysS)Cl_3^+$ (A – PBE0 functional; B – TPSS functional).

The calculated TD-DFT EAS of $Pd(H_4CysS)Cl_3^+$ was computed using two different density functionals: PBE0 and TPSS. Both spectra are shown in figure 7. The experimental spectrum has a maximum at 316 nm being only 1 nm different than predicted by PBE0 calculations (317 nm). The TPSS spectrum exhibits a larger difference from the experimental one, namely 10 nm. According to figure 7, the PBE0 density functional is more suitable for theoretical modeling of charge transfer transitions, while the TPSS one is better for theoretical modeling of d–d transitions (350–400 nm).

Table 5 shows contributions from different MOs to the electronic transition in $Pd(CysS)Cl_3^+$. The main electronic transition occurs from the H-5 MO to the LMO (PBE0) or from the H-7 MO to the LMO (TPSS). Figure 8 exhibits different MOs

Table 5. Contribution of different electronic charge transfers to the 317 nm absorbing band of $Pd(H_4CysS)Cl_3^+$.

Functional	λ_{exp} (eV)	λ_{Calcd} (eV)	f	MO	Transition
PBE0	3.914	3.924	0.087	H-7 → L (7.47%) H-5 → L (69.69%) H-3 → L (13.88%)	$\pi \rightarrow \pi^* +$ LMCT
TPSS	3.914	3.999	0.080	H-7 → L (46.71%) H-3 → L + 1 (16.13%)	$\pi \rightarrow \pi^* +$ MLCT + LMCT

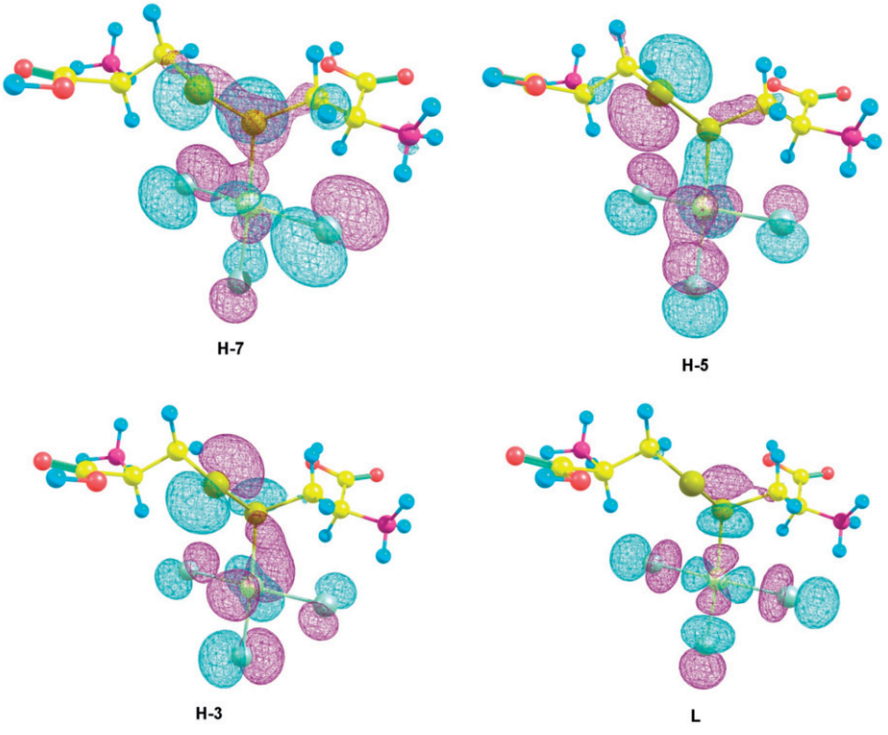

Figure 8. Visualized H-7, H-5, H-3, and L molecular orbitals of $Pd(H_4CysS)Cl_3^+$.

(PBE0) contributing to the 317 nm charge-transfer absorption band of $Pd(H_4CysS)Cl_3^+$. An atomic orbital population analysis (PBE0) is given in table 6. The TPSS data are enclosed as "Supplementary material": the molecular orbitals of $Pd(H_4CysS)Cl_3^+$ and their percentage composition.

Both PBE0 and TPSS calculations give evidence of $\pi \rightarrow \pi^*$ charge transfer from S1 ("free") to S2 ("coordinating") sulfur being the main contributor to the 316 nm absorption peak. Also, charge transfer occurs from the Cl^- (L′) 2p orbitals to the d_{z^2} orbital of Pd(II) in the Pd-cystine complex.

Table 6. Percentage composition of $Pd(H_4CysS)Cl_3^+$ molecular orbitals.

MO	Energy (eV)	Pd	S1	S2	3Cl
H-7	−8.563	–	2.41 $2p_x$ 2.05 $2p_y$	12.94 $2p_x$	7.00 $2p_x$ 25.62 $2p_y$ 12.39 $2p_z$
H-5	−7.995	5.50 d_{z^2} 13.75 d_{xy}	4.75 $2p_y$ 14.68 $2p_z$	–	26.67 $2p_z$
H-3	−7.644	6.47 $d_{x^2-y^2}$ 4.21 d_{z^2} 18.45 d_{xy} 8.15 d_{yz}	5.11 $2p_y$ 8.64 $2p_z$	–	16.372p_y 3.85 $2p_z$
L	−2.963	4.97 $d_{x^2-y^2}$ 23.00 d_{z^2} 8.00 d_{xy}	–	6.12 $2p_z$	9.06 $2p_x$ 7.54 $2p_y$ 8.20 $2p_z$

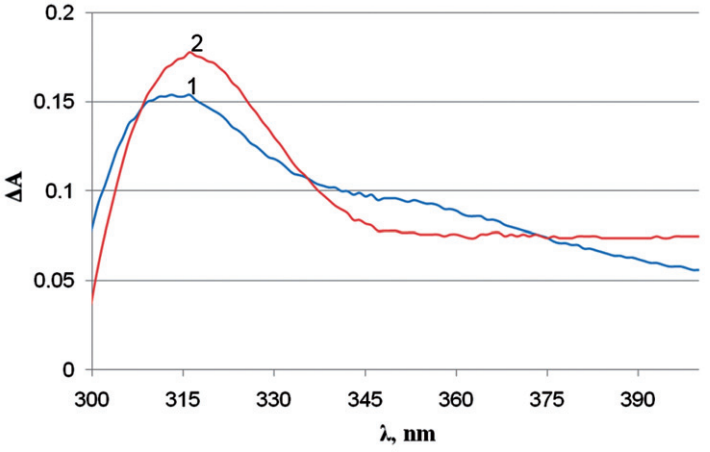

Figure 9. Plots of ΔA *vs.* λ for the $[PdCl_4]^{2-}$-H_3Cys^+ (1) and $[PdCl_4]^{2-}$-H_4CysS^{2+} (2) systems. $C_{Pd} = 2 \times 10^{-4}$ mol L^{-1}; $C_{CysS} = 2 \times 10^{-5}$ mol L^{-1}. $C_{Cys} = 4 \times 10^{-5}$ mol L^{-1}. $C_{HCl} = 0.5$ mol L^{-1}. $I = 0.5$. 298 K.

3.5. *Disulfide bond*

Pd(II) is known to initiate or to boost the fission of disulfide bonds and is widely used as catalyst in such reactions. An auxiliary experiment was carried out to ensure that no S–S bond fission occurred during the reaction of Pd(II) with cystine. Two solutions of $[PdCl_4]^{2-}$ were prepared: the one containing cysteine and the other containing cystine with $C_{Cys} : C_{CysS}$ ratio being 2 : 1.

The ΔA–λ plot (figure 9) for the $[PdCl_4]^{2-}$-cysteine system looked similar to the one for the $[PdCl_4]^{2-}$-cystine system but had its maximum at a different wavelength: 312 instead of 317 nm. Such shift, together with spectral differences beyond 340 nm, gave evidence that no S–S bond fission occurred during the reaction of $[PdCl_4]^{2-}$ with cystine.

S–S bond fission, if only this had occurred, would have led to cysteine formation in 2 : 1 ratio with respect to the cystine concentration. Protonation processes are very rapid, so H_3Cys^+ would be the reactive species under our conditions and $[H^+]$ would affect the complex formation parameters both in thermodynamic and kinetic studies. Since no $[H^+]$ effect on such parameters was found during our study, this is the second evidence that S–S bond fission does not take place.

4. Conclusions

- Complex formation of $[PdCl_4]^{2-}$ with L-cystine in hydrochloric acid solutions was studied for the first time. Thermodynamic parameters for the resulting complex formation have been determined (K_1, ΔH, and ΔS). Analysis of $[H^+]$ and $[Cl^-]$ effects on K_{app} clearly indicates monodentate S-coordination of cystine in $[Pd(H_4CysS)Cl_3]^+$.
- Kinetics of the $[PdCl_4]^{2-}$ reaction with L-cystine in hydrochloric acid solutions have also been studied for the first time. The complex-formation reaction is first order with respect to both Pd(II) and cystine; its second-order rate constant and activation parameters were determined.
- The experimental rate law was obtained including quantitative effects of the background components H^+ and Cl^-. The expression obtained is in good accordance with a theoretical model of the solvation mechanism pathway. Some discrepancies are explained by experimental errors and contribution from the direct substitution mechanism.
- The structure of $PdH_4CysSCl_3^+$ suggested from analysis of the thermodynamic data is verified and confirmed by quantum chemical (DFT/TD-DFT) calculations. Cystine coordination occurs *via* one sulfur of the disulfide group. The theoretical EAS (TD-DFT) contains an absorption band at 317 nm; the same is found in the experimental ΔA–λ plots.

Supplementary material

Raw spectral data (ΔA values) are used for intrinsic stability constant calculations. Cartesian coordinates for the DFT-optimized structures are shown in figure 8. Also reaction rate values, dependences of k_{obs} on temperature and C_{Pd} are provided. Molecular orbitals and their contributions to charge transfer in $Pd(H_4CysS)Cl_3^+$ are computed by the TD-DFT/TPSS method.

Acknowledgments

The authors thank the RF State Contracts No. 02.740.11.0269 and No. 02.740.11.0629 for their partial financial support. They also thank the SFU Super-computer Center for generous donation of CPU-time.

References

[1] J. Vicente, A. Arcas. *Coord. Chem. Rev.*, **249**, 1135 (2005).
[2] D.T. Richens. *Chem. Rev.*, **105**, 1961 (2005).
[3] S. Sakir, E. Bicer, O. Cakir. *Electrochem. Commun.*, **2**, 586 (2000).
[4] N.N. Golovnev, A.A. Leshok, G.V. Novikova. *Russ. J. Inorg. Chem.*, **55**, 291 (2010).
[5] S. Akerfeldt, G. Lwgren. *Anal. Biochem.*, **8**, 223 (1964).
[6] E.A. Al-Razaqa, N. Buttrusb, W. Al-Kattanb, A.A. Jbaraha, M. Almatarneha. *J. Sulfur Chem.*, **32**, 159 (2011).
[7] M.W. Schmidt, K.K. Baldridge, J.A. Boatz, S.T. Elbert, M.S. Gordon, J.H. Jensen, S. Koseki, N. Matsunaga, K.A. Nguyen, S. Su, T.L. Windus, M. Dupuis, J.A. Montgomery. *J. Comput. Chem.*, **14**, 1347 (1993).
[8] A.R. Allouche. *J. Comput. Chem.*, **32**, 174 (2011).
[9] G.A. Zhurko. *ChemCraft (Version 1.6)*. Available online at: http://www.chemcraftprog.com (accessed March 18, 2012).
[10] A.L. Tenderholt. *QMForge: A Program to Analyze Quantum Chemistry Calculations (Version 2.1)*Stanford University, Stanford, CA, USA (2007).
[11] L.I. Elding. *Inorg. Chim. Acta*, **6**, 647 (1972).
[12] L.I. Elding. *Inorg. Chim. Acta*, **6**, 683 (1972).
[13] F. Apruzzese, E. Bottari, M.R. Festa. *Talanta*, **56**, 459 (2002).
[14] E. Furia, M. Falvo, R. Porto. *J. Chem. Eng. Data*, **54**, 3037 (2009).
[15] J.H. Espenson. *Chemical Kinetics and Reaction Mechanisms*, 2nd Edn, McGraw-Hill Inc., New York (1995).
[16] N.M. Emanuel, D.G. Knorre. *Chemical Kinetics: Homogeneous Reactions*, Wiley (Halsted Press), New York (1973).
[17] K.A. Connors. *Chemical Kinetics, the Study of Reaction Rates in Solution*, VCH Publisher, New York (1990).
[18] D.J.A. De Waal, W. Robb. *Int. J. Chem. Kinet.*, **6**, 309 (1974).
[19] R.G. Wilkins. *Kinetics and Mechanism of Reactions of Transition Metal Complexes*, 2nd Edn, VCH Publisher, New York (1991).
[20] G.K. Rauth, S. Maity, C. Sinha. *Trans. Met. Chem.*, **28**, 518 (2003).
[21] M. Anbuchezhiyan, S. Ponnusamy, C. Muthamizhchelvan. *Physica B*, **405**, 1119 (2010).
[22] P. Heines, H.-L. Keller. *Z. Kristallogr. NCS*, **219**, 9 (2004).
[23] S. Nadeem, M.K. Rauf, S. Ahmad, M. Ebihara, S.A. Tirmizi, S.A. Bashir, A. Badshah. *Trans. Met. Chem.*, **34**, 197 (2009).